Electrical and Thermal Models of CNT TSV and Graphite Interface

Boris Vaisband, *Member, IEEE*, Ange Maurice, Chong Wei Tan, Beng Kang Tay, *Member, IEEE*, and Eby G. Friedman, *Fellow, IEEE*

***Abstract*— Carbon nanotubes (CNTs) are a suitable replacement for metals commonly used as a fill material for through substrate vias (TSVs). The electrical and thermal contact resistance, however, between the CNT TSVs and the horizontal metal interconnects (typically copper) can limit the use of CNT technology. A replacement for the horizontal metal interconnects in the form of graphite material is proposed in this paper. Electrical and thermal models of the interface between CNT TSVs and graphite interconnect are compared to the interface between CNT TSVs and copper interconnect. The proposed models include electrical and thermal crowding effects as well as the skin effect. The CNT/graphite interface exhibits up to 72.6% and 71.9%, respectively, lower electrical and thermal resistance as compared to the CNT/copper interface.**

***Index Terms*— 3-D IC, carbon nanotubes (CNTs), electrical model, graphite, thermal model, through substrate via (TSV).**

I. Introduction

A THROUGH substrate via (TSV) based three-dimensional (3-D) structure is an effective platform for heterogeneous integration. The integration of a wide range of circuits and materials is enabled within a 3-D platform. The TSVs are short vertical interconnections between layers (typically 20 μm in length and 2 to 4 μm in diameter [1]) that carry both electrical signals and heat (thermal TSVs) [1].

Thermal mitigation is of particular importance in 3-D ICs. Unlike in 2-D circuits, the thermal paths from the on-chip hot spots toward the heat sinks are congested by additional material layers. The heat is often trapped within the 3-D structure.

Manuscript received December 14, 2017; revised February 23, 2018; accepted March 1, 2018. Date of publication March 29, 2018; date of current version April 20, 2018. This work was supported in part by the Ministry of Education, Academic Research Fund, TIER 2, Singapore, under Grant MOE2014-T2-2-105, in part by the Binational Science Foundation under Grant 2012139, in part by the National Science Foundation under Grant CCF-1329374, Grant CCF-1526466, and Grant CNS-1548078, in part by IARPA under Grant W911NF-14-C-0089, and in part by Cisco Systems and Intel. The review of this paper was arranged by Editor M. S. Bakir. *(Corresponding author: Boris Vaisband.)*

B. Vaisband is with the Department of Electrical and Computer Engineering, University of California, Los Angeles, CA 90095 USA (e-mail: vaisband@ucla.edu).

A. Maurice, C. W. Tan, and B. K. Tay are with NOVITAS, Nanoelectronics Center of Excellence, School of Electrical and Electronic Engineering, Nanyang Technological University, Singapore 639798 (e-mail: maur0003@e.ntu.edu.sg; chongwei@ntu.edu.sg; ebktay@ntu.edu.sg).

E. G. Friedman is with the Department of Electrical and Computer Engineering, University of Rochester, Rochester, NY 14627 USA (e-mail: friedman@ece.rochester.edu).

Color versions of one or more of the figures in this paper are available online at http://ieeexplore.ieee.org.

Digital Object Identifier 10.1109/TED.2018.2812761

TABLE I
MAXIMUM CURRENT DENSITY AND THERMAL CONDUCTIVITY FOR DIFFERENT MATERIALS USED IN TSVS AND ON-CHIP INTERCONNECTS

Material	Maximum current density $[\frac{A}{cm^2}]$	Thermal conductivity $[\frac{W}{m \cdot K}]$
Copper	$1.5 \cdot 10^6$	400
Tungsten	$1 \cdot 10^6$	175
CNT bundle	$5 \cdot 10^9$	1,767
Graphite/MLG	$1 \cdot 10^8$	1,300

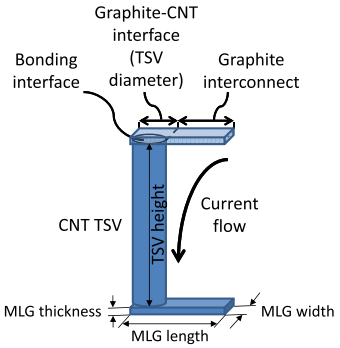

Fig. 1. CNT TSV connected to a graphite interconnect.

Different solutions have therefore been proposed to alleviate thermal congestion, ranging from algorithmic approaches (*i.e.*, thermal floorplanning and thermal TSV placement) [1] to microfluidic channels [2]. In this paper, the integration of highly thermally conductive materials is proposed.

Copper (Cu) and tungsten (W) are common TSV fill materials [1], and copper is commonly used for on-chip interconnects. The integration of carbon nanotubes (CNTs) as the fill material of TSVs, and graphite or multilayer graphene (MLG) as the horizontal interconnect material are proposed in this paper. Both CNTs and graphite are carbon-based materials that are highly thermally conductive, and can support three orders of magnitude higher current densities as compared to copper and tungsten [3]. The maximum current density and thermal conductivity of these materials are listed in Table I.

The integration of CNT TSVs and MLG interconnect is a promising technology for 3-D ICs. Little is known, however, concerning the properties at the interface between a vertical CNT bonded to a horizontal layer of graphite. Both electrical and thermal models describing this interface between CNT TSVs and graphite interconnect are proposed in this paper. The interface structure is shown in Fig. 1.

The rest of this paper is composed of the following sections. The electrical and thermal properties of CNTs, MLG, and the CNT/MLG interface are discussed in Section II. Electrical and thermal models of the CNT/MLG interface are described in Section III. A comparison of the CNT/MLG and CNT/Cu interfaces is discussed in Section IV. Some conclusions are offered in Section V.

II. Carbon-Based Material Properties

The electrical and thermal properties of carbon-based materials (MLG and CNT) are described in Sections II-A and II-B. The properties of the interface between CNTs and MLG are also reviewed in Section II-C.

A. Graphite Properties

A single layer of graphene exhibits a low electrical in-plane resistivity of 1.4 $\mu\Omega \cdot$ cm [4]. Nevertheless, the resistance of graphene on a substrate is significantly greater than copper. Graphite is therefore an effective horizontal interconnect material.

Although graphite exhibits poor in-plane resistivity (318 $\mu\Omega \cdot$ cm) as compared to graphene, intercalation doping with different compounds can significantly lower the in-plane resistivity of graphite [5]. The experimental evaluation of graphite with intercalation compounds of AsF_5 and SbF_5 exhibits an in-plane resistivity of up to 1 $\mu\Omega \cdot$ cm [5]. The intercalation of graphite increases the electrical anisotropy of the material. Assuming a horizontal graphite interconnect intercalated with AsF_5, the resistance in the vertical direction is six orders of magnitude greater than in the horizontal (in-plane) direction [6]. The electrical anisotropy of the proposed structure significantly affects the current flowing within the graphite at the interface with the TSV (see Fig. 1).

Graphite exhibits a thermal in-plane conductivity of 1300 (W/m $\cdot$ K) (see Table I); intercalated graphite, however, exhibits a lower thermal in-plane conductivity of 700 (W/m $\cdot$ K) [7], approximately twice greater than Cu. As compared to copper interconnect, this property improves the heat flow from the 3-D structure to the surroundings. The electrical and thermal properties of intercalated graphite are listed in Table II. Note, since graphite intercalation is typically used to lower the resistivity of graphite, the term graphite (or MLG) is used here to describe intercalated graphite.

A thickness (t) of 0.5 μm for the graphite and Cu interconnects is used (the resistance of both graphite and Cu interconnects scale similarly with reduced thickness). The number of graphene layers is therefore $N = t/_{0.34}$ nm (the thickness of a single graphene layer is 0.34 nm), approximately 1470.

B. Single-Wall CNT TSV

In this paper, TSVs are composed of a bundle of single-wall CNTs (SWCNTs). To characterize the material properties of SWCNT bundles, the properties of an isolated SWCNT are first individually described. From [8], the impedance of a SWCNT is

$$Z_{\text{SWCNT}} = R_Q + R_S + j\omega L_{K,\text{CNT}} \tag{1}$$

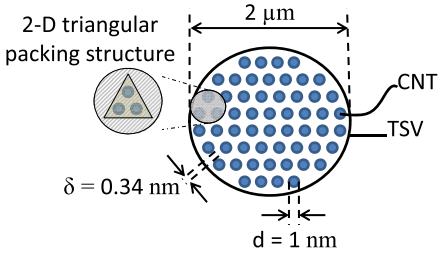

Fig. 2. Top view of CNT TSV. The diameter of the CNT and TSV is, respectively, 1 nm and 2 μm. δ = 0.34 nm is the minimum Van der Waals spacing between a pair of CNTs [9]. The area per CNT is based on a 2-D triangular packing structure [10].

where $R_Q = h/2q^2$ is the quantum ballistic resistance, $R_S = h \cdot H/2q^2\lambda$ is the scattering resistance, and $L_{K,\text{CNT}} = h \cdot H/4q^2 v_F$ is the kinetic inductance originating from the inertia of the electron mass. h is the Planck constant, H is the TSV height, q is the electron charge, v_F is the fermi velocity ($8 \cdot 10^5$ m/s), and λ is the mean free path of the electrons ($\lambda \approx 1$ μm). Substituting these expressions into (1) yields

$$Z_{\text{SWCNT}} = \frac{h}{2q^2}\left(1 + \frac{H}{\lambda} + j\omega\frac{H}{2v_F}\right). \tag{2}$$

To determine the complex effective impedance of a bundle Z_B, an estimate of the number of SWCNTs N_{CNT} within a bundle is necessary. The arrangement of the CNT ropes in a 2-D triangular packing structure, as illustrated in Fig. 2, has been experimentally demonstrated [10]. The number of CNTs within a bundle is, therefore,

$$N_{\text{CNT}} = \frac{2\pi R_{\text{TSV}}^2}{\sqrt{3}(d+\delta)^2} \tag{3}$$

where d is the diameter of an SWCNT, δ is the minimum Van der Waals intertube spacing, and R_{TSV} is the radius of the TSV. From (3), the bundle impedance is

$$Z_B = \frac{Z_{\text{SWCNT}}}{N_{\text{CNT}} F_m}. \tag{4}$$

The metallic fraction of CNTs F_m describes the effective number of conducting TSVs within an SWCNT bundle. Statistically, one third of the CNTs are metallic ($F_m = 1/3$); however, the chirality of the CNTs can be tuned to obtain a higher metallic fraction ($F_m = 0.91$) [11]. The effective resistivity of the CNT bundle is extracted from Z_B.

In terms of heat transport, the chirality of the CNTs does not significantly affect the thermal conductance [12]. The effective thermal conductivity of a CNT bundle K_B is, therefore,

$$K_B = K_{\text{CNT}} N_{\text{CNT}} \left(\frac{r}{R_{\text{TSV}}}\right)^2, \tag{5}$$

where K_{CNT} is the thermal conductivity of an isolated SWCNT and r is the radius of a nanotube ($d/2$).

The effective resistivity and thermal conductivity of a CNT bundle are strongly dependent on the density of the CNTs. High-density CNTs should therefore be maintained within the bundle to provide a greater electrical and thermal conductivity than Cu or W TSVs. The highest reported density of vertically aligned nanotubes is $1.5 \cdot 10^{13}$ CNT/cm^2 [13]. The maximum

theoretical density is $6.43 \cdot 10^{13}$ CNT/cm^2. Reducing the gap between the experimental and theoretical maximum density of CNTs is a major challenge that can be solved by improving CNT synthesis methods.

C. Interface Between CNTs and MLG

Covalent bonding between CNTs and graphene is thermodynamically stable [14]. Most of the existing works focus on 3-D architectures, *i.e.,* pillared graphene, consisting of CNT pillars connecting graphene sheets. Pillared graphene is primarily used in energy storage and supercapacitor applications [14]. Due to the covalent nature of the junction and the similar material, the scattering of phonons and electrons is greatly reduced, resulting in higher conduction at the interface. The junction properties are assumed to be similar to the properties of a grain boundary (GB) [15] in a planar graphene sheet.

The effective thermal surface conductivity G_Q^{th} of an SWCNT bundle is determined from the thermal surface conductivity between a single CNT and a graphene layer (G_J)

$$G_Q^{\text{th}} = \frac{G_J \cdot d \cdot t \cdot N_{\text{CNT}}}{{R_{\text{TSV}}}^2}, \tag{6}$$

where t is the thickness of the nanotube wall ($t = 0.34$ nm). The quality of the bond at the interface may affect the electrical and thermal properties at the interface. The carbon atoms at the interface may not be perfectly bonded, partly due to crystallographic mismatch or experimental fluctuations. Both high- and low-quality interfaces are discussed here to consider the breadth of possibilities. For example, the thermal surface conductance (G_J), assuming strong sp^2 covalent bonding at the interface, is 13 GW/(m^2 · K). In weak Van der Waals bonds, G_J is 25 MW/(m^2 · K). The end of the CNT only exhibits physical adsorption on the graphene plane [16]. From (6), for a 1-μm TSV, the thermal resistance at the interface ranges from 35 to 18 500 K/W. The thermal surface conductance of the CNT/graphite interface is $G_Q^{\text{th}} = 8\,930$ MW/(m^2 · K) (~3572 times higher than the CNT/copper interface [17]).

The effective surface resistivity of the interface ρ_Q is determined from the 1-D GB resistivity ρ_{GB}

$$\rho_Q = \frac{\rho_{\text{GB}} {R_{\text{TSV}}}^2}{N_{\text{CNT}} \cdot d}. \tag{7}$$

In [15], the resistivity of the GB (ρ_{GB}) is shown to range from 500 to 35 000 Ω · μm depending upon the quality of the GB. From (7), for a 1-μm TSV, the electrical resistance at the interface ranges from 78 m Ω to 5.51 Ω, consistent with previously reported experimental measurements [18]. The assumption that the CNT/graphite junction acts as a GB is therefore supported. The electrical surface resistivity of CNT/graphite is $\rho_Q = 0.24\ \Omega \cdot \mu\text{m}^2$ (~42 times lower than the CNT/copper interface [19]).

III. Interface Models

Electrical and thermal models of the interface between CNT TSV and MLG interconnects are described in this section. Electrical phenomena such as current crowding and the anisotropy of the resistivity have been incorporated within the electrical model. The skin effect at high frequencies is also included in the model. In addition, the heat crowding effect is included within the thermal model.

A. Electrical Model

The electrical model at the interface between a CNT TSV and graphite interconnect includes the resistance of the MLG interconnect above the TSV (R_{intMLG}) and the resistance associated with the covalent bond between the MLG and CNT materials (R_{intQ}).

Two parameters are required to accurately determine R_{intMLG}: 1) current crowding p^{cc}, and 2) anisotropy p^a. For homogeneous metals, the sheet resistance of an interconnect bend is ~0.45 of the sheet resistance of a straight piece of interconnect due to current crowding [20]. This behavior, however, is not the case with CNT and MLG interconnects due to the different resistivity and cross-sectional area of the conductors. A second parameter p^a is introduced by the anisotropy of the graphite which significantly affects the path of the charge carriers. It is assumed here that current crowding and anisotropy are independent of each other (as verified by simulation).

The resistance of the graphite interconnect above the TSV (see Fig. 1) is

$$R_{\text{intMLG}} = \rho_{\text{MLG}} \frac{l_{\text{MLG}} \cdot p^{cc} \cdot p^a}{A_{\text{MLG}}}, \tag{8}$$

where ρ_{MLG} is the in-plane resistivity of graphite, and A_{MLG} and l_{MLG} are, respectively, the cross-sectional area and length of the graphite interconnect above the interface. The resistance of MLG R_{intMLG} exhibits a linear relationship with both p^{cc} and p^a.

Unlike the resistivity of the graphite above the TSV, R_{intQ} is based on the quality of the covalent bond between the CNTs and MLG. The resistance of the bond is, therefore,

$$R_{\text{intQ}} = \rho_Q \frac{1}{A_{\text{int}}}, \tag{9}$$

where ρ_Q is the resistivity of the interface as determined from the covalent bond between the CNT and MLG materials, and A_{int} is the cross-sectional area of the interface.

A model of the interface resistance is provided by combining (8) and (9),

$$\begin{aligned} R_{\text{int}} &= R_{\text{intMLG}} + R_{\text{intQ}} \\ &= \rho_{\text{MLG}} \frac{l_{\text{MLG}} \cdot p^{cc} \cdot p^a}{A_{\text{MLG}}} + \rho_Q \frac{1}{A_{\text{int}}}. \end{aligned} \tag{10}$$

This model is evaluated in Section IV using COMSOL Multiphysics [21] simulations.

B. Thermal Model

The interface between the CNTs and graphite is thin; therefore, the thermal capacitance is neglected and only the thermal resistance is considered. The interface is, therefore, modeled as two thermal resistors in series (similar to the electrical model). The first resistor $R_{\text{intMLG}}^{\text{th}}$ considers the thermal resistance of

TABLE II
COMSOL MODEL PARAMETERS OF THE CNT TSV WITH GRAPHITE HORIZONTAL INTERCONNECT. DIMENSIONS ILLUSTRATED IN FIG. 1

Parameter	Value
Geometric	
TSV radius	0.5 to 2.5 μm
TSV height	20 μm
MLG thickness	0.5 μm
MLG width	1 to 5 μm
MLG length	10 μm
Electrical	
CNT in-plane resistivity	$6.17{\cdot}10^{-8}$ Ω·m
MLG in-plane resistivity	$1.1{\cdot}10^{-8}$ Ω·m
CNT/MLG interface surface resistivity	$0.24{\cdot}10^{-12}$ Ω·m^2
Anisotropy	10^6
Thermal	
CNT in-plane conductivity	1,750 W/(m·K)
MLG in-plane conductivity	700 W/(m·K)
CNT/MLG interface surface conductivity	8,930 MW/(m^2·K)
Anisotropy	10^3

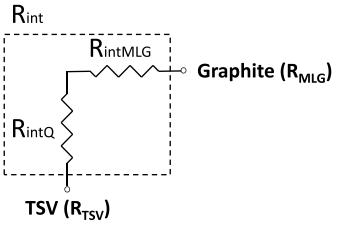

Fig. 3. Schematic of the evaluated structure.

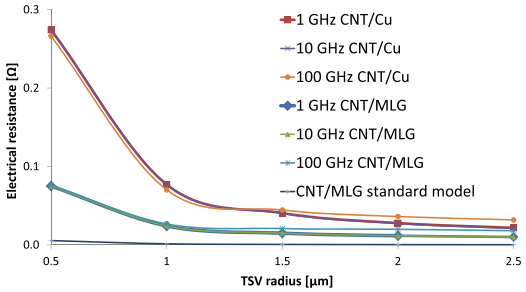

Fig. 4. Comparison of electrical resistance at the CNT/MLG and CNT/Cu interfaces.

the graphite material above the interface. The second thermal resistor $R^{\text{th}}_{\text{intQ}}$ considers the thermal resistance due to the quality of the covalent bond between the CNTs and the graphite.

Similar to electrical current, more heat flows in the less thermally resistive path. A similar effect to current crowding, therefore, occurs and is included in the thermal model. This effect is modeled using a heat crowding parameter p^{hc}. The thermal anisotropy of graphite is 10^3 (Table II). From simulations, the effect of anisotropy on the conduction of heat within the proposed structure is negligible; anisotropy is, therefore, ignored in the thermal model.

From (6), the thermal resistance is

$$R^{\text{th}}_{\text{int}} = \rho^{\text{th}}_{\text{MLG}} \frac{l_{\text{MLG}} \cdot p^{hc}}{A_{\text{MLG}}} + \left(G^{\text{th}}_{Q} \cdot A_{\text{int}}\right)^{-1}, \tag{11}$$

where A_{int} is the area of the interface.

IV. EVALUATION OF INTERFACE MODELS

A structure consisting of a CNT TSV and two MLG interconnects connected at each end of the TSV has been evaluated using COMSOL. A comparison between the CNT/MLG and CNT/Cu structures is provided, permitting the different model parameters to be extracted. The geometric, electrical, and thermal parameters of the evaluated model are listed in Table II.

A. Electrical Evaluation

The separate components of the complete structure are serially connected, as depicted in Fig. 3; therefore, the total resistance is the sum of the partial resistances. Unlike the separate components, the resistance of the complete structure (R_{full}) includes the resistance of the MLG at the interface (R_{intMLG}) and the effects of current crowding. The complete structure is therefore compared with the sum of the individual components, permitting the resistance of the interface to be determined.

The difference between the resistance of the complete structure and the combined resistance of the individual components is the interface resistance,

$$R_{\text{intMLG}} = 0.5 \cdot (R_{\text{full}} - (R_{\text{TSV}} + 2 \cdot R_{\text{MLG}})). \tag{12}$$

Note that R_{intQ} is only dependent on the quality of the bond between the CNTs and graphite. R_{intQ} has therefore been omitted in the evaluation of R_{intMLG}.

The resistance of the interface, including a comparison to copper interconnect, is shown in Fig. 4. For larger TSVs ($R_{\text{TSV}} > 1.4\ \mu$m), the resistance described by Fig. 4 increases with frequency due to the skin effect. The CNT/MLG structure exhibits up to 72.6% lower resistance than the CNT/Cu structure for all evaluated frequencies. The resistance of the CNT/MLG interface is determined from the standard model $R = \rho(l/A)$, assuming the resistivity listed in Table II. The resistance of the standard model is smaller by up to 98.8% than the resistance obtained from simulation since current crowding is not considered in the standard model.

From (8), assuming $p^a = 1$ (*i.e.,* an isotropic material), the current crowding parameter p^{cc} is

$$p_{cc} = \frac{R_{\text{intMLG}} \cdot A_{\text{intMLG}}}{\rho_{\text{intMLG}} \cdot l_{\text{intMLG}}}. \tag{13}$$

p^{cc} is assumed to be independent of p^a. This assumption simplifies the extraction of the current crowding parameter.

The current crowding parameter as a function of frequency is shown in Fig. 5. The current crowding parameter p^{cc} increases with frequency due to the skin effect. The eddy currents formed at high frequencies enhance the current crowding phenomenon by pushing the charge carriers toward the shell of the conductor.

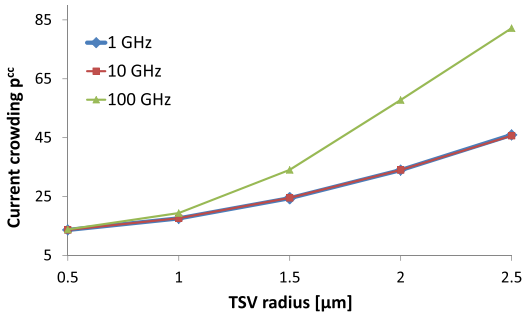

Fig. 5. Current crowding parameter p^{cc} at different frequencies, 1, 10, and 100 GHz.

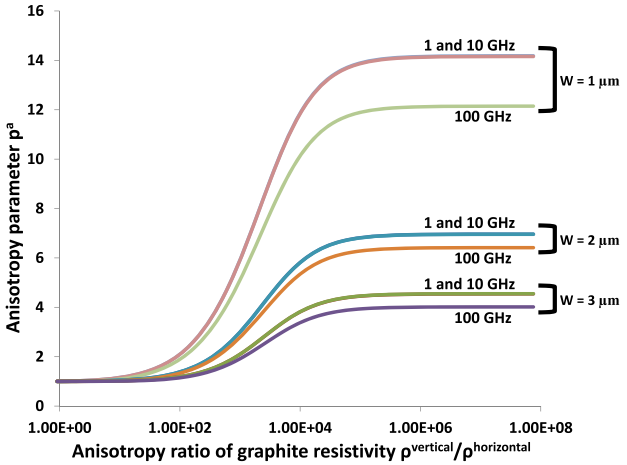

Fig. 6. Anisotropy parameter p^{cc} as a function of the ratio of the vertical and horizontal resistivities for graphite widths (the diameter of the TSV) of 1, 2, and 3 μm. Note that the curves for 1 and 10 GHz overlap.

The anisotropy parameter p^a is extracted from (8) by setting p^{cc} for each frequency according to the following expression,

$$p^a = \frac{R_{\text{intMLG}} \cdot A_{\text{intMLG}}}{\rho_{\text{intMLG}} \cdot l_{\text{intMLG}} \cdot p^{cc}(f)}. \tag{14}$$

The anisotropy parameter p^a is evaluated for different widths of graphite, ranging from 1 to 3 μm, as shown in Fig. 6.

From Fig. 6, the anisotropy parameter exhibits certain trends within three regions. Region 1: constant at low anisotropy ratio (approximately up to 10). Region 2: increasing at medium anisotropy ratio (approximately from 10 to 10^5). Region 3: constant at high anisotropy ratio (ranging from approximately 10^5 to 10^8). This behavior is expected with anisotropic materials such as graphite. For a low anisotropy ratio (region 1), the graphite behaves similar to metal where the charge carriers are free to move in all directions within the conductor; specifically, between the graphene layers of the MLG. For the medium range anisotropy ratio (region 2), the charge carriers are limited to the lower/upper sheets of graphene (in the top/bottom MLG interconnect shown in Fig. 1), increasing the resistance of the graphite. At high anisotropy ratios (region 3), the charge carriers are confined to the bottom sheet of the graphene within the MLG. Any further increase in the anisotropy ratio does not increase the resistance of the conductor since all of the charge carriers preferentially flow at the bottom of the graphite interconnect.

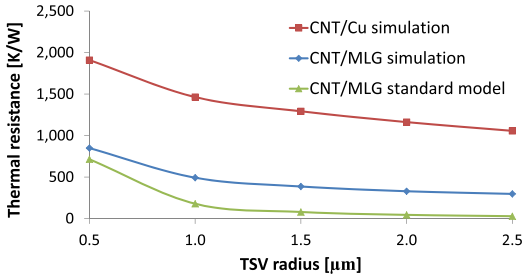

Fig. 7. Comparison of thermal resistance at the interface for CNT/MLG and CNT/Cu.

The dependence of the frequency and width of p^a is also shown in Fig. 6. An increase in the width of the conductor exhibits an expected effect, *i.e.*, the anisotropy ratio has a reduced effect on the anisotropy parameter due to the lower resistance of the graphite. The increased frequency, however, reveals an unexpected phenomenon where the skin effect reduces the resistance of the conductor at high anisotropy ratios. This behavior is caused by the eddy currents within the conductor pushing the charge carriers to the top and bottom layers of the MLG. The anisotropy limits the charge to flow only within the bottom layer as the path from the top to bottom layer becomes highly resistive. Fabrication of lower anisotropy graphite will greatly reduce the interface resistance.

To account for R_{intQ} in the proposed electrical model, a range of contact resistivities at the interface has been evaluated since the quality of the covalent bond between the CNTs and graphite can differ significantly, as described in Section II-C. A contact resistance is included within the electrical model at the interface, as described by (9). The simulated interface resistance is consistent with R_{intQ} at the interface in the form of a higher resistivity within the relevant range of resistance (from 78.6 mΩ to 5.5 Ω).

B. Thermal Evaluation

The thermal model is similar to the electrical model (thermal resistors replace electrical resistors in Fig. 3). The sum of the thermal resistance of the individual components of the structure is subtracted from the thermal resistance of the complete structure, $R^{\text{th}}_{\text{intMLG}} = 0.5 \cdot (R^{\text{th}}_{\text{full}} - (R^{\text{th}}_{\text{TSV}} + 2 \cdot R^{\text{th}}_{\text{MLG}}))$, resulting in the thermal resistance of the interface between the CNTs and the graphite. This model is based on the series behavior of thermal resistances (similar to the electrical resistance).

To determine the thermal resistance, the heat flux needs to be ascertained. The following expression describes the thermal resistance [22],

$$R^{\text{th}} = \frac{\Delta T}{Q}, \tag{15}$$

where ΔT is the temperature difference across a heat conducting structure and Q is the heat transfer rate. A COMSOL simulation of the thermal resistance at the interface is shown in Fig. 7. A comparison between the MLG and Cu

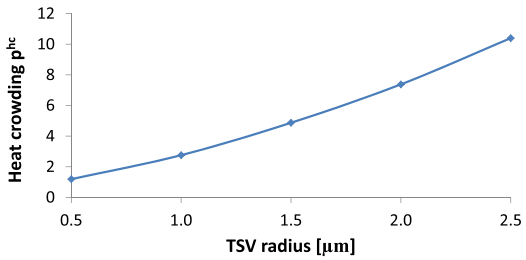

Fig. 8. Heat crowding parameter p^{hc} as a function of the TSV radius.

interconnects is also depicted in Fig. 7. The CNT/MLG interface exhibits up to 71.9% lower thermal resistance than the CNT/Cu interface. Similar to p^{cc}, the heat crowding parameter is

$$p_{hc} = \frac{R^{\text{th}}_{\text{intMLG}} \cdot A_{\text{intMLG}}}{\rho^{\text{th}}_{\text{intMLG}} \cdot l_{\text{intMLG}}}. \tag{16}$$

The heat crowding parameter p^{hc}, extracted from the thermal resistance, is illustrated in Fig. 8. Similar to the current crowding parameter (in Fig. 5), p^{hc} increases with the radius of the TSV. The heat crowding phenomenon becomes more significant in wide conductors since the thermal resistance of the longer heat flow path also increases. p^{hc} compares well with the theoretical evaluation of heat spreading in [23]. The thermal resistance ($R^{\text{th}}_{\text{intMLG}}$), depicted in Fig. 7, is obtained from the standard model $R^{\text{th}} = (1/k) \cdot (l/A)$, where k is the thermal conductivity of the material (from Table II), and l and A are, respectively, the length and cross-sectional area of the thermal conductor (the graphite/CNT interface shown in Fig. 1). The thermal resistance of the standard model is smaller by up to 90.4% than the thermal resistance obtained from simulation since the heat crowding parameter is not considered by the standard model.

A thermal contact resistance has been added to the thermal model at the interface between the CNT TSV and the horizontal graphite interconnect in the form of an increased thermal resistivity. Similar to the electrical model, the evaluation of $R^{\text{th}}_{\text{intQ}}$ is consistent with including the thermal resistance (ranging from 35 to 18 500 K/W) at the interface.

V. Conclusion

Electrical and thermal models of the interface between a CNT TSV and graphite interconnect are presented here. The electrical characteristics of the CNTs, graphite, and CNT/MLG interface are also reviewed. The proposed models are validated using COMSOL simulations. The electrical and thermal resistance of a CNT/MLG and a CNT/Cu structures are compared. The CNT/MLG interface exhibits lower electrical and thermal resistance by up to, respectively, 72.6% and 71.9%.

The CNT/MLG interface models are also compared to theoretical values. Including current and heat crowding effects in the electrical and thermal models of the CNT/MLG interface enhances the accuracy of the proposed models by up to, respectively, 98.8% and 90.4%.

References

[1] V. F. Pavlidis, I. Savidis, and E. G. Friedman, *Three-Dimensional Integrated Circuit Design*, 2nd ed. San Mateo, CA, USA: Morgan Kaufmann, 2017.

[2] H. Mizunuma, Y.-C. Lu, and C.-L. Yang, "Thermal modeling and analysis for 3-D ICs with integrated microchannel cooling," *IEEE Trans. Comput.-Aided Des. Integr. Circuits Syst.*, vol. 30, no. 9, pp. 1293–1306, Sep. 2011.

[3] C. Subramaniam *et al.*, "One hundred fold increase in current carrying capacity in a carbon nanotube–copper composite," *Nature Commun.*, vol. 4, p. 2202, Jul. 2013.

[4] X.-Y. Fang, X.-X. Yu, H.-M. Zheng, H.-B. Jin, L. Wang, and M.-S. Cao, "Temperature- and thickness-dependent electrical conductivity of few-layer graphene and graphene nanosheets," *Phys. Lett. A*, vol. 379, no. 37, pp. 2245–2251, Oct. 2015.

[5] F. L. Vogel, "The electrical conductivity of graphite intercalated with superacid fluorides: Experiments with antimony pentafluoride," *J. Mater. Sci.*, vol. 12, no. 5, pp. 982–986, May 1977.

[6] E. McRae, J. F. Mareché, M. Lelaurain, G. Furdin, and A. Herold, "Conductivity anisotropy in AsF_5—intercalated graphite," *J. Phys. Chem. Solids*, vol. 48, no. 10, pp. 957–963, Oct. 1987.

[7] J. Heremans, J.-P. Issi, I. Zabala-Martinez, M. Shayegan, and M. Dresselhaus, "Thermoelectric properties of a dilute graphite donor intercalation compound," *Phys. Lett. A*, vol. 84, no. 7, pp. 387–389, Aug. 1981.

[8] C. Xu, H. Li, R. Suaya, and K. Banerjee, "Compact AC modeling and performance analysis of through-silicon vias in 3-D ICs," *IEEE Trans. Electron Devices*, vol. 57, no. 12, pp. 3405–3417, Dec. 2010.

[9] B. T. Kelly, *Physics of Graphite*. Englewood, NJ, USA: Applied Science London, 1981.

[10] A. Thess *et al.*, "Crystalline ropes of metallic carbon nanotubes," *Science*, vol. 273, no. 5274, pp. 483–487, Jul. 1996.

[11] A. R. Harutyunyan *et al.*, "Preferential growth of single-walled carbon nanotubes with metallic conductivity," *Science*, vol. 326, no. 5949, pp. 116–120, Oct. 2009.

[12] T. Yamamoto, S. Watanabe, and K. Watanabe, "Universal features of quantized thermal conductance of carbon nanotubes," *Phys. Rev. Lett.*, vol. 92, no. 7, p. 075502, Feb. 2004.

[13] G. Zhong, J. H. Warner, M. Fouquet, A. W. Robertson, B. Chen, and J. Robertson, "Growth of ultrahigh density single-walled carbon nanotube forests by improved catalyst design," *ACS Nano*, vol. 6, no. 4, pp. 2893–2903, Mar. 2012.

[14] G. K. Dimitrakakis, E. Tylianakis, and G. E. Froudakis, "Pillared graphene: A new 3-D network nanostructure for enhanced hydrogen storage," *ACS Nano Lett.*, vol. 8, no. 10, pp. 3166–3170, Sep. 2008.

[15] A. W. Tsen *et al.*, "Tailoring electrical transport across grain boundaries in polycrystalline graphene," *Science*, vol. 336, no. 6085, pp. 1143–1146, Jun. 2012.

[16] J. Shi, Y. Dong, T. Fisher, and X. Ruan, "Thermal transport across carbon nanotube-graphene covalent and Van Der Waals junctions," *J. Appl. Phys.*, vol. 118, no. 4, pp. 044302-1–044302-7, Jul. 2015.

[17] J. Xu and T. S. Fisher, "Enhanced thermal contact conductance using carbon nanotube array interfaces," *IEEE Trans. Compon. Packag. Technol.*, vol. 29, no. 2, pp. 261–267, Jun. 2010.

[18] Y. Zhu *et al.*, "A seamless three-dimensional carbon nanotube graphene hybrid material," *Nature Commun.*, vol. 3, p. 1225, Nov. 2012.

[19] N. Chiodarelli *et al.*, "Integration of vertical carbon nanotube bundles for interconnects," *J. Electrochem. Soc.*, vol. 157, no. 10, pp. K211–K217, Oct. 2010.

[20] M. Horowitz and R. W. Dutton, "Resistance extraction from mask layout data," *IEEE Trans. Comput.-Aided Des. Integr. Circuits Syst.*, vol. CAD-2, no. 3, pp. 145–150, Jul. 1983.

[21] (2013). *COMSOL Multiphysics 5.0*. [Online]. Available: http://www.comsol.com/

[22] B. Vaisband, I. Savidis, and E. G. Friedman, "Thermal conduction path analysis in 3-D ICs," in *Proc. IEEE Symp. Circuits Syst.*, Jun. 2014, pp. 594–597.

[23] S. Lee, S. Song, V. Au, and K. P. Moran, "Constricon/spreading resistance model for electronics packaging," in *Proc. ASME/JSME Thermal Eng. Joint Conf.*, Mar. 1995, pp. 199–206.

Boris Vaisband (S'12–M'17) is currently a Post-Doctoral Scholar with the Center for Heterogeneous Integration and Performance Scaling, University of California, Los Angeles, CA, USA. From 2008 to 2011, he held a hardware design position at Intel. In 2013 and 2015, he interned with Cisco Systems and Google, respectively. His current research interests include integration of heterogeneous systems, power delivery, and thermal aware design and floorplanning.

Ange Maurice received the M.Eng. degree in materials sciences from the Institut National des Sciences appliquées, Lyon, France, in 2014. He is currently pursuing the Ph.D. degree with the School of Electrical and Electronic Engineering, NOVITAS, Nanyang Technological University, Singapore.

His current research interests include the study of 2-D materials resistive devices, femtosecond laser irradiation, silicon oxide memories, and thermal management in electronic devices.

Chong Wei Tan is currently a Post-Doctoral Research Fellow with the School of Electrical and Electronic Engineering, NOVITAS, Nanyang Technological University, Singapore. His current research interests include carbon-based hybrid materials for MEMS and nano-electronics applications, thermal management in electronic devices, advanced 3-D interconnect TSV, diamond as substrate for high power devices and carbon nanotubes for field emission, and RF applications.

Beng Kang Tay (M'93) is a Full Professor with the School of Electrical and Electronic Engineering, Nanyang Technological University, Singapore, and currently the Deputy Director of the CNRS International NTU Thales Research Alliance. His research interests include thin film technology especially in graphene, tetrahedral amorphous carbon, metal oxides, nanocomposites, and carbon nanotubes. His research team received the ASEAN Outstanding Engineering Award and the National Technology Award in 1997 and 2000, respectively.

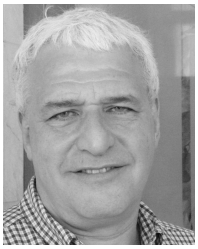

Eby G. Friedman (F'00) is currently a Distinguished Professor with the University of Rochester, Rochester, NY, USA, and a Visiting Professor with the Technion-Israel Institute of Technology, Haifa, Israel. He has authored over 500 papers, book chapters, and patents, and 18 books in the fields of high speed and low power CMOS circuits, 3-D integration, and synchronous clock and power delivery.

Dr. Friedman is a Senior Fulbright Fellow.